Theoretical Studies of Inorganic and Organometallic Reaction Mechanisms. 11. Migratory Insertion of Coordinated Nitric Oxide into Cobalt−Carbon Bonds

Shuqiang Niu and Michael B. Hall*

Contribution from the Department of Chemistry, Texas A&M University, College Station, Texas 77843

Received June 13, 1996. Revised Manuscript Received December 4, 1996[⊗]

Abstract: The migratory insertion reaction of NO into the Co−CH$_3$ σ-bond in the cobalt cyclopentadienyl complex CpCo(NO)(CH$_3$) (**2**), both with and without the assistance of an incoming ligand (PH$_3$, **1**), has been studied using ab initio molecular orbital and density functional theory (DFT) methods. The insertion without PH$_3$ association (Mechanism I) occurs with an activation energy of 10−20 kcal/mol, and the intermediate, CpCoN(O)CH$_3$ (**3a**), forms with an endothermicity of 8−17 kcal/mol at the DFT-B3LYP and coupled cluster with singles and doubles (CCSD) levels of theory. The overall reaction to the product, CpCoN(O)CH$_3$(PH$_3$) (**5b**), was exothermic by −10 to −16 kcal/mol depending on the level of theory. An alternative mechanism II which begins with PH$_3$ association and NO bending is endothermic by 16−18 kcal/mol and is immediately followed by a NO insertion barrier of 19−34 kcal/mol for an overall barrier of 35−52 kcal/mol. Therefore, Mechanism I is the favored pathway. This result is in very good agreement with the kinetic experiments of Weiner and Bergman. Charge density and Laplacian analysis at the RHF level and the MO analysis from extended Hückel calculations reveal that the Co center plays a dual, electron acceptor and donor, role in the migratory insertion for both Mechanisms I and II. For Mechanism I the better acceptor and donor character of the metal center results in a lower activation energy as it cycles from a d^8 (18e$^-$) complex at **2** to a d^8 (16e$^-$) intermediate at **3** and back to a d^8 (18e$^-$) product at **5**. In contrast, for Mechanism II the original σ$_{Co-C}$ orbital must rise to high energy before it can transfer charge density to the d$_{xz}$ orbital of the product as it cycles from a d^8 (18e$^-$) complex at **2** to a d^6 (18e$^-$) intermediate (**4**) and back to a d^8 (18e$^-$) complex at **5**, a cycle which consequently requires a greater activation energy.

Introduction

Nitric oxide, a very versatile molecule and ligand, has become one of the most fascinating entities in neuroscience and immunology.[1] This increased attention to the biochemistry of NO and has prompted interest in its organometallic chemistry.[2] In particular, the migratory insertion of NO into transition metal−carbon bonds, an important reaction in metal nitrosyl complexes, may be important in biochemical reactions.

It is well-known that migratory insertion of CO into transition-metal−carbon bonds is a critical step in many important carbon−carbon bond forming processes involving homogeneous transition-metal catalysts.[3] There have been numerous experimental and theoretical studies of the classical reaction 1.[4−11]

$$Mn(CO)_5CH_3 + CO \rightarrow Mn(CO)_5(C(O)CH_3) \quad (1)$$

Calculations, at various levels from extended Hückel calculations[6,7] through other approximate calculations[8,9] to ab initio, configuration-interaction studies,[5,10,11] show that in this migra-

tory-insertion reaction the CH$_3$ ligand migrates to a bound CO followed by the additional CO taking up the empty coordination site.

In contrast, investigations into the migratory-insertion reaction of NO into the metal−carbon bond are more limited.[6a] In the case of reaction 2

$$CpCr(NO)_2(CH_3) + NO^+ \rightarrow CpCr(NO)_2(N(O)CH_3)^+ \quad (2)$$
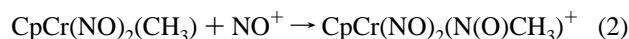
Legzdins and co-workers suggest an external attack of NO$^+$ on methyl to explain the insertion process.[12] In the insertion of NO into a cluster-carbon bond, Vollhardt and co-workers also suggest an intermolecular insertion process.[13] However, in the insertion reaction of NO into the Co−CH$_3$ bond as shown in reaction 3

$$CpCo(NO)(CH_3) + PPh_3 \rightarrow CpCo(PPh_3)(N(O)CH_3) \quad (3)$$
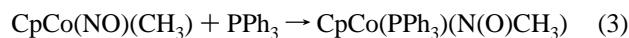
labeling experiments and kinetic measurements by Weiner and Bergman[14] show an intramolecular insertion process and suggest

⊗ Abstract published in *Advance ACS Abstracts,* March 1, 1997.

(1) (a) Culotta, E.; Koshland, D. E., Jr. *Science* **1992,** *258,* 1862. (b) Feldman, P. L.; Griffith, O. W.; Stuehr, D. J. *C&E* **1993,** *71*(5), 26.

(2) Richter-Addo, G. B.; Legzdins, P. *Metal Nitrosyls*; Oxford University Press: New York, 1992.

(3) (a) Parshall, G. W. *Homogeneous Catalysis*; Wiley: New York, 1880. (b) Elschenbroich, C.; Salzer, A. *Organometallics*; VCH Publishers: New York, 1989. (c) Koga, N.; Morokuma, K. *Chem. Rev.* **1991,** *91,* 823.

(4) (a) Kuhlmann, E. K.; Alexander, J. J. *J. Coord. Chem. Rev.* **1980,** *33,* 195. (b) Kurfee, L. D.; Rothwell, I. P. *Chem. Rev.* **1988,** *88,* 1059.

(5) Axe, F. U.; Marynick, D. S. *J. Am. Chem. Soc.* **1988,** *110,* 3728.

(6) (a) Berke, H.; Hoffmann, R. J. *J. Am. Chem. Soc.* **1978,** *100,* 7224. (b) Hoffmann, P.; Stauffert, P.; Tatsumi, K.; Nakamura, A.; Hoffmann, R. *Organometallics* **1985,** *4,* 404. (c) Hoffmann, P.; Stauffert, P.; Tatsumi, K.; Nakamura, A.; Hoffmann, R. *J. Am. Chem. Soc.* **1985,** *107,* 4440.

(7) Curtis, M. D.; Shiu, K.-B.; Butler, W. M. *J. Am. Chem. Soc.* **1986,** *108,* 1550.

(8) Ziegler, T.; Versluis, L.; Tschinke, V. *J. Am. Chem. Soc.* **1986,** *108,* 612.

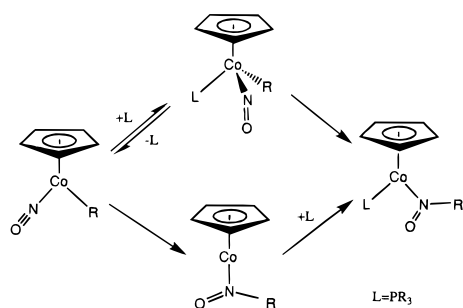(9) Axe, F. U.; Marynick, D. S. *Organometallics* **1987,** *6,* 572.

(10) (a) Sakaki, S.; Kitaura, K.; Morokuma, K.; Ohkabo, K. *J. Am. Chem. Soc.* **1983,** *105,* 2280. (b) Koga, N.; Morokuma, K. *J. Am. Chem. Soc.* **1985,** *107,* 7230.

(11) Rappé, A. K. *J. Am. Chem. Soc.* **1987,** *109,* 5605.

(12) Legzdins, P.; Wassink, B.; Einstein, F. W. B.; Willis, A. C. *J. Am. Chem. Soc.* **1986,** *108,* 317.

(13) Goldhaber, A.; Vollhart, K. P. C.; Walborsky, E. C.; Wolfgruber, M. *J. Am. Chem. Soc.* **1986,** *108,* 516.

Scheme 1

that this system proceeds through methyl migration followed by phosphine addition as illustrate in the bottom of Scheme 1. Obviously, this mechanism is similar to that of the CO insertion reaction 1.[4]

Prompted by Weiner and Bergman's experimental works, several important questions have raised concerning this mechanism. First, as distinct from CO, nitric oxide is a more versatile ligand; it can function as either a $3e^-$ ligand or an $1e^-$ ligand. Thus, a bent M−NO structure could lead to another reaction pathway as shown in the top of Scheme 1. As it is well-known that bent NO plays an important role in providing a low energy path in other reactions,[15] one might wonder why it does not in this case.

In this work, the migratory-insertion reaction of NO into the Co−CH_3 bond with and without phosphine association (Scheme 1) is investigated with the density functional theory (DFT) and ab initio molecular orbital theory. The geomerties and energies of the reactants, intermediates, transition states, and products are determined by the DFT method, and the reaction energies are recalculated at the coupled cluster with singles and doubles (CCSD) method. A qualitative description of the electron structural changes along each of these reaction paths is developed through both RHF charge density analysis (ρ) and extended Hückel (EH) Walsh diagrams.

Computational Details

Effective core potentials (ECPs) were employed in all ab initio and DFT[16] calculations. In the ECPs for Co, the 3s and 3p orbitals were treated explicitly along with the 3d, 4s, and 4p valence orbitals. The ECP basis set of Co were described with the double-ζ basis (541/41/41) of Hay and Wadt.[17] For carbon, nitrogen, oxygen, and phosphorus, the ECPs and basis sets of Stevens, Basch, and Krauss[18] were used in double-ζ form. [He] and [Ne] configurations were taken as cores for the first and second row main group atoms, respectively. The Dunning-Huzinaga (31) double-ζ basis set was used for the hydrogen atom.[19] In our ab initio calculations we replaced the phosphine group in the actual molecules by PH_3.[15]

In previous work[20] we have shown (i) that the RHF method is inadequate for the study of these reactions with first-row transition metals; (ii) that a near degeneracy problem associated with the NO ligand not only destroys the accuracy of the geometry optimizations at the MP2 level but also energy calculations at even higher levels

(MPX);[21] (iii) that the DFT-B3LYP method[22,23] gives a reliable description of the geometries and a fair discription of the relative energies in this first-row transition metal system, (iv) that nonperturbative method such as CCSD[24] are required in ab initio studies, and (v) that polarization functions make a relatively small contribution to the relative energy for this system. Thus, geometries of the reactants, intermediates, transition states, and products were fully optimized at the DFT levels. Becke's three parameter hybrid method[22] and the Lee−Yang−Parr correlation functional[23] (B3LYP) were employed in all DFT calculations. In general, the transition states (TS) were characterized by calculating the Hessian matrix and determining the number of imaginary frequency.[25]

For a direct estimation of electron correlation effects and accurate reaction energetics, CCSD calculations were carried out with geometries optimized at the DFT level. In the CCSD calculations all electrons were included in the correlation energy calculation.

All ab initio calculations were performed with GAMESS-UK,[26] GAUSSIAN92, and GAUSSIAN94 programs,[27] at the Cornell Theory Center on IBM ES6000 and Scalable Powerparallel (SP2), at the Supercomputer Center of Texas A&M University and the Department of Chemistry on Silicon Graphics Power Challenge servers, and on Silicon Graphic Power Indigo II workstations in our laboratory and at the Institute of Scientific Computation (ISC) of Texas A&M University.

Extended Hückel calculations[28] were carried out with CACHe program using parameters collected by S. Alvarez.[29] All geometrical parameters of EH calculations have been taken from the ab initio optimized structures. The topological analysis of the Laplacian of the charge density was performed with MOPLOT.[30]

Results and Discussion

The two possible pathways for the NO insertion reaction are shown in Scheme 1. One path begins with the migratory-insertion of a linear NO followed by the coordination of PR_3 (see Mechanism I). The other path begins with attack of PR_3, the bending of the NO, and ends with the migratory-insertion

(14) (a) Weiner, W. P.; White, M. A.; Bergman, R. G. *J. Am. Chem. Soc.* **1981**, *103*, 3612. (b) Seidler, M. D.; Bergman, R. G. *Organomet.* **1983**, *2*, 1897. (c) Weiner, W. P.; Bergman, R. G. *J. Am. Chem. Soc.* **1983**, *105*, 3922.

(15) (a) Song, J.; Hall, M. B. *J. Am. Chem. Soc.* **1993**, *115*, 327. (b) Sulfab, Y.; Basolo, F.; Rheingold, A. L. *Organomet.* **1989**, *8*, 2139.

(16) Parr, R. G.; Yang, W. *Density-functional theory of atoms and molecules*; Oxford University Press: Oxford, 1989.

(17) Hay, P. J.; Wadt, W. R. *J. Chem. Phys.* **1985**, *82*, 299.

(18) Stevens, W. J.; Basch, H.; Krauss, M. *J. Chem. Phys.* **1984**, *81*, 6026.

(19) (a) Huzinaga, S. *J. Chem. Phys.* **1965**, *42*, 1293. (b) Dunning, T. H., Jr. *J. Chem. Phys.* **1970**, *53*, 2823.

(20) Niu, S.-Q.; Hall, M. B. *J. Phys. Chem. A* **1997**, *101*, 1360.

(21) (a) Møller, C.; Plesset, M. S. *Phys. Rev.* **1936**, *46*, 618. (b) Pople, J. A.; Binkley, J. S.; Seeger, R. *Int. J. Quantum Chem.* **1976**, *S10*, 1.

(22) (a) Becke, A. D. *Phys. Rev.* **1988**, *A38*, 3098. (b) Becke, A. D. *J. Chem. Phys.* **1993**, *98*, 1372. (c) Becke, A. D. *J. Chem. Phys.* **1993**, *98*, 5648.

(23) Lee, C.; Yang, W.; Parr, R. G. *Phys. Rev.* **1988**, *B37*, 785.

(24) (a) Bartlett, R. J. *Ann. Rev. Phys. Chem.* **1981**, *32*, 359. (b) Scuseria, G. E.; Schaefer, III H. F. *J. Chem. Phys.* **1989**, *90*, 3700.

(25) (a) Schlegel, H. B. *Theor. Chim. Acta* **1984**, *66*, 33. (b) Foresman, J. B.; Frish, Æ. *Exploring Chemistry with Electronic Structure Methods*; Gaussian, Inc.: 1993.

(26) Guest, M. F.; Kendrick, J.; van Lenthe, J. H.; Schoeffel, K.; Sherwood, P. GAMESS-UK; Daresbury Laboratory: Warrington, WA4 4AD, U.K., 1994.

(27) Frisch, M. J.; Trucks, G. W.; Schlegel, H. B.; Gill, P. M. W.; Johnson, B. G.; Robb, M. A.; Cheeseman, J. R.; Keith, T. A.; Petersson, G. A.; Montgomery, J. A.; Raghavachari, K.; Al-Laham, M. A.; Zakrzewski, V. G.; Ortiz, J. V.; Foresman, J. B.; Cioslowski, J.; Stefanov, B. B.; Nanayakkara, A.; Challacombe, M.; Peng, C. Y.; Ayala, P. Y.; Chen, W.; Wong, M. W.; Andres, J. L.; Replogle, E. S.; Gomperts, R.; Martin, R. L.; Fox, D. J.; Binkley, J. S.; Defrees, D. J.; Baker, J.; Stewart, J. P.; Head-Gordon, M.; Gonzalez, C.; Pople, J. A. Gaussian 94 (Revision A. 1); Gaussian, Inc.: Pittsburgh, PA, 1995.

(28) Hoffmann, R. *J. Chem. Phys.* **1963**, *39*, 1397.

(29) (a) CACHe Scientific (Release 3.5), Inc. Copyright 1993. (b) Alvarez, S. *Table of Parameters for Extended Hückel Calculations*; Universitat de Barcelona, June 1989.

(30) (a) Interactive MOPLOT: A package for the interactive display and analysis of molecular wave functions in corporating the program MOPLOT (Lichtenburger, D), PLOTDEN (Bader, R. F. W.; Kenworthy, D. J.; Beddal, P. M.; Runtz, G. R.; Anderson, S. G.), SCHUSS (Bader, R. F. W.; Runtz, G. R.; Anderson, S. G.; Biegler-Koenig, F. W.), and EXTREM (Bader, R. F. W.; Biegler-Koenig, F. W.), Sherwood, P.; MacDougall, P. J. 1989. (b) Bader, R. F. W. *Atoms in Molecules: A Quantum Theory*; Oxford University Press: New York, 1990. (c) A (3,−1) critical point means that two curvatures of the Laplacian ($\nabla^2\rho$) of ρ are negative (ρ is a maximum at this point) along two axes in the corresponding plane and a curvature is positive (ρ is a minimum at this point) along the third axis which is perpendicular to this plane. A (3,+1) critical point means that two curvatures of the Laplacian ($\nabla^2\rho$) of ρ are positive (ρ is a minimum at this point) along two axes in the corresponding plane and a curvature is negative (ρ is a maximum at this point) along the third axis which is perpendicular to this plane.

(see Mechansim II). We will consider and examine these two mechanisms separately.

Mechanism I: Migratory-Insertion of NO into the Co−C σ Bond Followed by PH$_3$ Association. Structures. In this section, we will examine Mechanism I in which an unsaturated η^1-methylnitrosocomplex (**3a**) is directly formed from a methyl nitrosyl complex (**2**). The ligand, PH$_3$ (**1**), is not involved in the initial migratory-insertion transition state but enters the coordination sphere later as shown in Mechanism I. The reaction from **3a** to **5b** can proceed via two distinct pathways: (i) rotation of the nitroso ligand around Co−N bond (or swinging the nitroso ligand) to the η^2-methylnitrosocomplex (**3b**) followed by PH$_3$ association and (ii) PH$_3$ association to form **5a** followed by rotation of the nitroso ligand around the Co−N bond.

Mechanism I
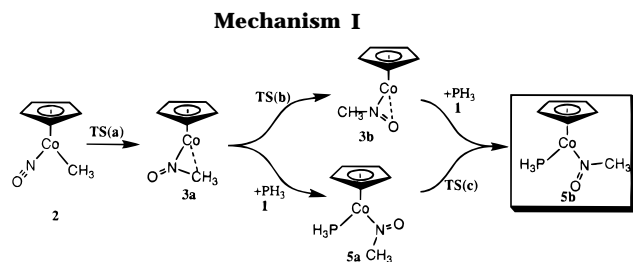
The DFT-B3LYP optimized geometries of **2**, **TS(a)**, **3a**, **TS(b)**, and **3b** are illustrated in Figure 1. In the reactant (**2**) the metal center coordinates nitric oxide to form a linear Co−N−O nitrosyl methyl complex. It is notable that the Co−N distance in **2** is shorter by 0.09 Å than that in η^1-methylnitrosocomplex (**3a**) (see Figure 1) and the N−O distance in **2** is longer by 0.10 Å than that calculated for NO$^+$. These significant differences suggest strong multiple bonding interaction between the Co and N atoms (Co=N=O) in **2**, arising from the σ donor and strong π acceptor character of the nitrosyl ligand.

In the transition state, **TS(a)**, as the nitrosyl group bends, the Co−CH$_3$ bond is breaking and the N−CH$_3$ bond is forming. The Co−CH$_3$, Co−N, and N−O distances are longer by 0.21, 0.03, and 0.03 Å than those of the reactant (**2**), respectively, while the N−CH$_3$ distance is shorter by 0.71 Å than that in **2**. Thus, the migration of the methyl group dominates in this step (**2** to **TS(a)**).

In the η^1-intermediate (**3a**), the nitrosyl group is now bent, the N−CH$_3$ bond has formed, and Co−CH$_3$ bond has broken completely. It is noteworthy that the N−CH$_3$ bond is still longer by 0.04 Å than the B3LYP optimized N−C single bond (1.514 Å) as calculated for the product (**5b**). The B3LYP Co−N−CH$_3$ angle (93.2°) is obviously smaller than the expected value for sp^2-hybridization (120°) and the inside C−H bond is longer by 0.018 Å than the B3LYP optimized C−H bond as calculated in **5b**. Such structural features point to the presence of a Co−H−C β-agostic interaction[31] in **3a**, where the N−C bond is also lengthened by this interaction.

Structures **3b** and **5b** differ from their isomers **3a** and **5a** by a rotation of the nitroso-group around the Co−N bond (see Figures 1 and 4). Figure 1 shows that (i) the N−O bond of **3b** is longer by 0.10 Å than that of **3a** and (ii) the Co−N−O angle in **3b** is smaller by 64.3° than that in **3a**. This Co−N−O angle is 29.3° larger than the expected value (120°) in **3a** and 35.0° smaller than the expected value in **3b**. Whereas **3a** shows an agostic Co−H−C interaction, **3b** shows a Co−O−N three-center interaction. The stronger Co−O−N three-center interaction results from the stabilization of **3b** as shown in Scheme 2, where the remnants of the in-phase π^* of NO acts as a π acceptor from Co. In contrast, there is no obvious Co−H−C and Co−O−N three-center interactions in the products **5a** and
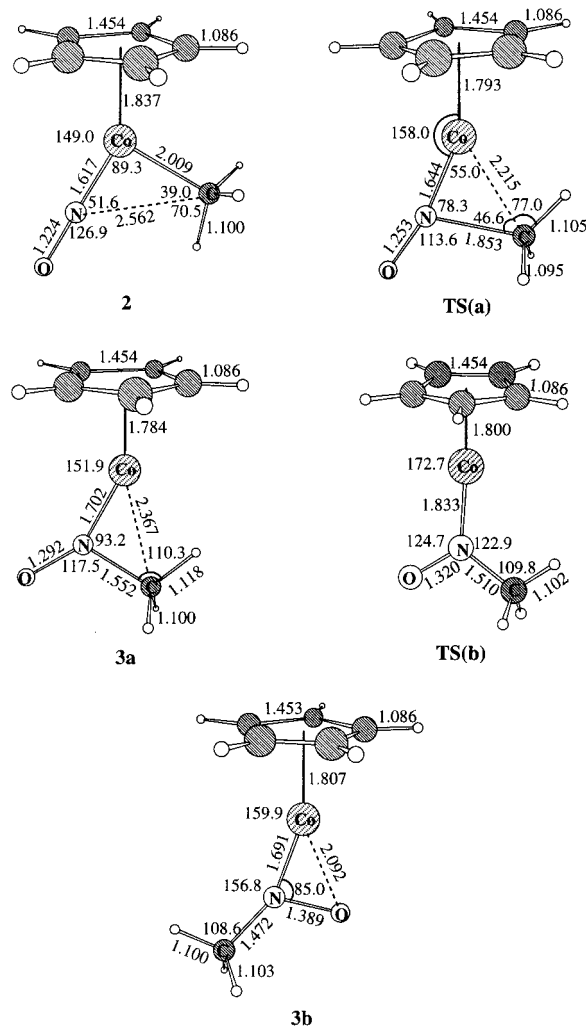

Figure 1. The DFT-B3LYP optimized geometries of the reactant **2**, transition states **TS(a)** and **TS(b)**, η^1-intermediate **3a**, and η^2-intermediate **3b** (only the average C−C and C−H distances be given for the Cp ring).

5b, respectively. The major factor contributing to the stabilization of **5a** and **5b** in the dative interaction between PH$_3$ and metal center which replaces the weaker interactions described above for **3a** and **3b**. Despite careful search for both the rotating and swinging barriers, we can find only one transition state **TS(b)** from **3a** to **3b**. The Cp−Co−N angle of **TS(b)** is nearby linear (172°), and the Co−N distance is longer by 0.13 Å than **3a**. Between **5a** and **5b** we found a rotational transition state, **TS(c)**, in which the Cp−Co−N−O dihedral angle is −79.5°.

Bonding. To provide a description of the changing bonds in the migratory-insertion step, the charge density has been analyzed along the reaction pathway by examining density ρ and Laplacian $\nabla^2\rho$ (Figure 2). The values of ρ and $\nabla^2\rho$ at the critical points, where $\vec{\nabla}\rho = 0$, are shown in Table 1. Contour plots of $\nabla^2\rho$ exhibits regions of local charge concentration, where $\nabla^2\rho < 0$ (dashed contours), and local charge depletion, where $\nabla^2\rho > 0$ (solid contours), respectively. According to the topological analysis of the density,[30b] a chemical bond is characterized by a (3,−1), "bond" critical point of the Laplacian ($\nabla^2\rho$) between the bonding nuclei; a site of nucleophilic attack or a structure characteristic of a ring is often characterized by a (3,+1) "ring" critical point.[30b,c] When $\nabla^2\rho > 0$, the bonding interaction at a (3,−1) critical point is characterized as a *closed-shell interaction* (ionic and hydrogen bonds); when $\nabla^2\rho < 0$, the bonding interaction at a (3,−1) critical point is characterized as a *shared interaction* (covalent bond). Thus, the positions and magnitudes of the local charge concentration and depletion
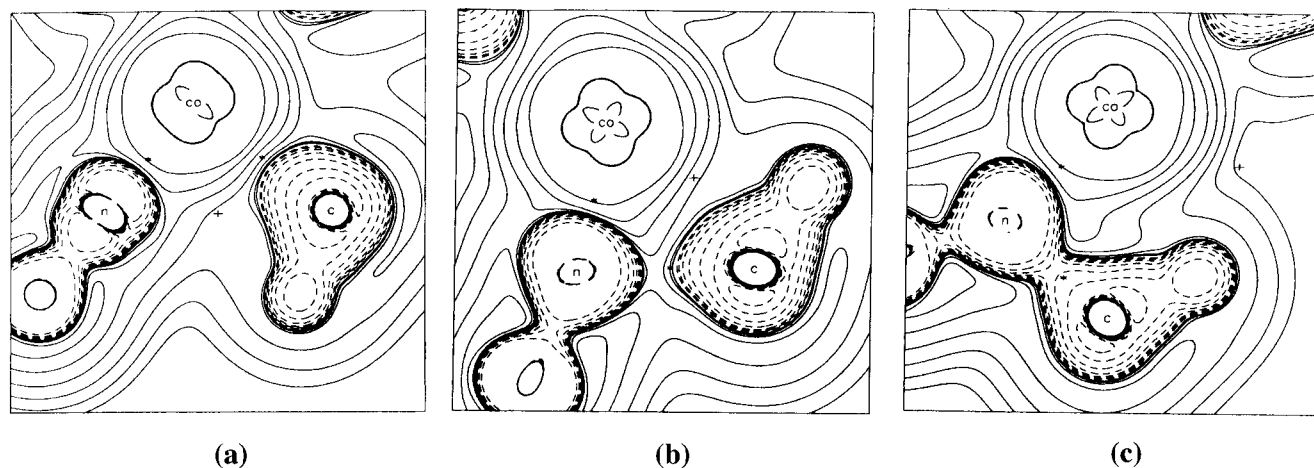
Figure 2. Contour plots of $\nabla^2\rho$ for the three structures along Mechanism I: (a) **2**, (b) **TS(a)**, and (c) **3a**. Seven geometric contours of each sign are plotted. The heights of adjacent contours differ by a factor 2. The absolute value of the largest contour is 1.00 au. The $(3,-1)$ and $(3,+1)$ critical points are indicated by stars and crosses, respectively.
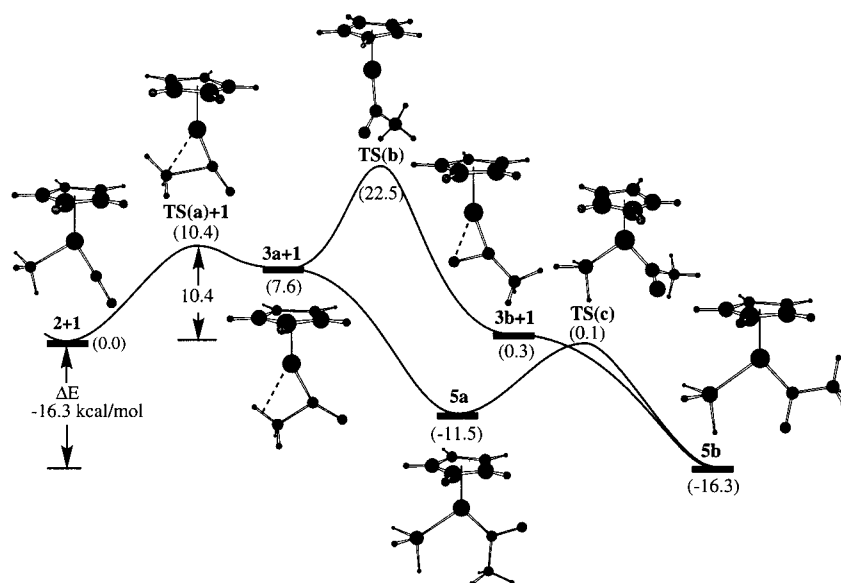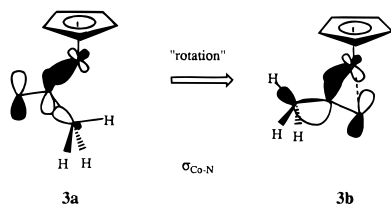

Figure 3. The profiles of the potential energy surfaces at the DFT-B3LYP level for Mechanism I (CCSD energies are given in Table 2).

Scheme 2

and these values at the critical points enable one to predict the bonding character and reactive sites within a molecule.

In Figure 2a, the Laplacian of the charge density for **2** has the characteristic d^8 "dumbbell" shape around Co. There are $(3,-1)$ bond critical points along the Co$-$NO and Co$-$CH$_3$ bond paths, while there is a $(3,+1)$ ring critical point between the N and methyl ligand. The ring critical point shows a position of charge depletion which is susceptible to attack by a nucleophile, here the lone pair at the N or C atom. Compared with **2**, the Laplacian of the charge density of **TS(a)** (Figure 2b) has switched the bond critical point of the Co$-$C bond for a ring critical point and the ring critical point between the N and C atoms to a bond critical point. The positive value of $\nabla^2\rho$ at the $(3,-1)$ critical point along the N$-$CH$_3$ bond path suggests that the atoms are linked by closed-shell interaction (dative bond). A charge density analysis of **2** and **TS(a)** at the RHF level (see Table 1) shows that the charge densities of the

Table 1. The Charge Density (ρ) on the Atoms[a] and Critical Points[b] and Laplacian of the Charge Density ($\nabla^2\rho$) at the Critical Point between the Bonded Atoms[b] Involved in Mechanism I

	2		**TS(a)**		**3a**	
	ρ	$\nabla^2\rho$	ρ	$\nabla^2\rho$	ρ	$\nabla^2\rho$
Co	16.292		16.505		16.511	
N	5.253		5.141		5.150	
C	4.595		4.318		4.207	
O	6.203		6.310		6.298	
Co$-$N	0.201	1.127	0.189	1.110	0.164	0.967
Co$-$C	0.104	0.142	0.041	*0.164*	0.007	*0.013*
N$-$C	0.037	*0.102*	0.116	0.030	0.206	$-$0.311
N$-$O	0.444	$-$0.959	0.419	$-$0.701	0.380	$-$0.442

[a] Mulliken charge density at the RHF level for the atom, in which the core electrons are not included (units at the atomic sites are electrons). [b] The values of $\nabla^2\rho$ at the $(3,+1)$ ring critical point are given in italic underline characters, other points are $(3,-1)$ bond critical points (units of ρ = e/au^3 and $\nabla^2\rho$ = e/au^5).

N and C (methyl) atoms decrease by 0.112 and 0.277 with respect to **2**, respectively, while the charge densities of the Co and O atoms increase by 0.213 and 0.107. The charge densities at the critical points of the N$-$O and Co$-$C bonds decrease by 0.025 and 0.063 with respect to **2**, respectively, while the charge density at the critical point between the N and C atoms increases by 0.080. However, the charge density at the critical point of the Co$-$N bond is changed very slightly. Thus, as the nitrosyl

Table 2. Relative Energies at the DFT-B3LYP and CCSD//B3LYP Levels for Reactants, Intermediates, Transition States, and Products via Mechanisms I and II (kcal/mol)

|	DFT	CCSD//DFT	Δ
1+2	0.00	0.00	0.00
1+TS(a)	10.38	19.54	9.16
1+3a	7.59	16.73	9.14
1+TS(b)	22.49	30.87	8.38
1+3b	0.34	6.32	5.98
4	15.65	18.00	2.35
TS(d)	34.68	52.12	17.44
5a	−11.46	−4.51	6.95
TS(c)	0.13	6.93	6.80
5b	−16.27	−9.76	6.51

group bends and the methyl ligand migrates, charge density is transferred from the C (methyl), N atoms, and Co−C, N−O bonds to the Co, O atoms, and the N−C bond. This observation is consistent with the need to transfer the Co−C lone pair to the metal center rather than directly to the N−C bond.

In Figure 2c, the Laplacian of the charge density for **3a** now shows a stronger shared interaction (covalent bond) along N−CH$_3$ bond path where the value of $\nabla^2\rho$ at the (3,−1) critical point is now negative. A ring critical point now appears beyond Co−N−CH$_3$ region in a position where it can be attacked by PH$_3$. Compared with **2**, the decrease in the absolute values of $\nabla^2\rho$ at the bond critical points of the Co−N and N−O bond of **3a**, 0.16 and 0.52, respectively (see Table 1), suggests that the strong multiple bonding interaction between the Co and N atoms (Co=N=O) of **2** has been diminished in **3a**. In the late stage of the reaction (**TS(a)** to **3a**), the charge densities at the C (methyl) atom and at the critical points of the Co−C, Co−N, and N−O bonds decrease by 0.111, 0.034, 0.026, and 0.039, respectively, while the charge density at the critical point of the N−C bond increases by 0.089. However, the charge densities of the Co and N atoms are nearly unchanged. Thus, the charge density transfers from the C atom (methyl), Co−N, and N−O bond to the N−C bond, and the Co and N atoms play an electron transfer role. Overall, along Mechanism I the N−C bond is formed and the Co−C bond is broken, the Co and N atoms play a dual role as electron acceptor and donor, while the C (methyl) atom plays a donor role, as shown in Scheme 3.

Energies. The profile of the potential energy surfaces for Mechanism I is presented in Figure 3. Energies at the DFT-B3LYP and CCSD levels for the reactants (**1** and **2**), intermediates (**3a** and **3b**), transition states (**TS(a)**−(**c**)), and products (**5a** and **5b**) via Mechanism I are shown in Table 2. In our discussion we will present both energy differences with the DFT-B3LYP value followed by the CCSD value. Note that the CCSD values for the relative energy are consistently larger than those of DFT (see Δ in Table 2, correlation coefficient = 0.956) in part because CCSD predicts the reactant (**2**) to be more stable. The activation barrier of the migratory-insertion step (**2** to **3a**) is calculated to be 10.4 and 19.5 kcal/mol. The migratory-insertion step **2** → **3a** is endothermic by 7.6 and 16.7 kcal/mol. The calculated results are in very good agreement with the observed activation enthalpy values for L$_n$(CH$_3$)M−CO to L$_n$M−C(O)CH$_3$ (M = Mn, Fe), 16.6−18.2 kcal/mol,[32] and the endothermicities obtained from ab initio calculations for L$_n$RM−CO to L$_n$M−C(O)R, 8.8−18.0 kcal/mol.[3c] The η^2-intermediate **3b** is more stable by 7.2 and 10.4 kcal/mol than the isomer **3a**; the swinging barrier from **3a** to **3b** is 14.9 and 14.1 kcal/mol. Despite careful search, we found no associative barriers from **3a** to **5a** or from **3b** to **5b**. One can safely say that the association of the phosphine to form the final nitrosomethyl complex occurs without a barrier. The product **5b** is more stable by 4.8 and 5.3 kcal/mol than the isomer **5a**, and the

rotational barrier from **5a** to **5b** is 11.6 and 11.0 kcal/mol. It has been suggested that the stable nitrosoalkane complex might be structure **5b** because of the steric effect between the migrated alkyl group and bulky phosphines.[4] Our results with the small PH$_3$ suggest that there is an electronic origin for the stability of **5b** over **5a**. The overall reaction was exothermic with a Δ*E* of −16.3 and −9.8 kcal/mol. These values are in very good agreement with the experimental enthalpy (Δ*H$_1$* = −13.0 kcal/mol) of reaction 1.[33] It is obvious that in Mechanism I the reaction happens in the presence of PH$_3$ along **2** → **TS(a)** → **3a** → **5a** → **TS(c)** → **5b**, and the migratory insertion is the rate-determining step.

Mechanism II: Migratory-Insertion of NO into the Co−C σ Bond Occurs After PH$_3$ Association. Structures. In this section we consider Mechanism II in which a bent-nitrosyl adduct (with PH$_3$) **4** forms first and then NO undergoes migratory insertion into the Co−C σ-bond to give product **5**. If the formation of **5** from **4** occurs directly, **5a** and **5b** should be alternative product geometries from the same insertion transition state **TS(d)**. However, it appears that **TS(d)** actually leads to **TS(c)**, the transition state for rotation of N(O)CH$_3$ ligand which converts **5a** to **5b**. The DFT-B3LYP optimized geometries of the 18e$^−$ intermediate (**4**), insertion transition state (**TS(d)**), rotation transition state (**TS(c)**), product (**5a**), and product (**5b**) are shown in Figure 4.

Mechanism II
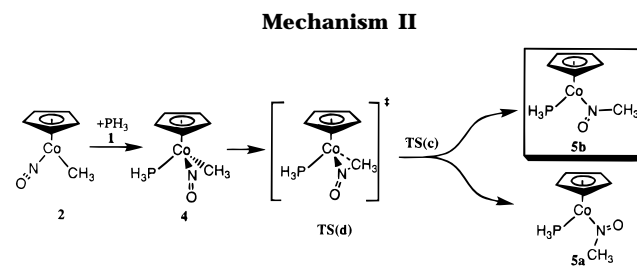
In the intermediate (**4**) the coordinated NO group has adopted a bent geometry. The Co−N−O angle is 125.4°. Compared with the reactant (**2**), the Co−N, N−O, and Co−Cp distances in **4** are longer by 0.16, 0.03, and 0.13 Å, respectively. The distortion of the nitrosyl group and association of the PH$_3$ group lead to a new 18e$^−$ complex that is clearly different from the other 18e$^−$ complexes **2** and **5** because of its longer Cp−Co distance (0.12−0.13 Å). In the insertion transition state, **TS(d)**, the N−O bond of the nitrosyl has been lengthened by 0.04 Å with respect to the bent-nitrosyl intermediate (**4**). Comparing other aspects of **4** with **TS(d)**, we find that the "forming" N−CH$_3$ bond is shorter by 1.2 Å, the "breaking" Co−CH$_3$ bond is longer by 0.28 Å, the CH$_3$−Co−Cp−P dihedral angle increases by 56.1°, and the N−Co−Cp−P dihedral angle increases by 6.4°. Thus, at the DFT-B3LYP level, the primary motion involves the CH$_3$ ligand. The geometric features of the products (**5a**, **5b**) and rotation transition state (**TS(c)**) have been discussed above.

Bonding. The Laplacian ($\nabla^2\rho$) contours of the charge density and the values of ρ and $\nabla^2\rho$ at the critical points along the migratory-insertion step are shown in Figure 5 and Table 3. In Figure 5a the Laplacian of the charge density for **4** shows a "four-leaf" clover shape typical of d^6 metal centers. Again, there are (3,−1) bond critical points along the Co−NO and Co−CH$_3$ bond paths, while there is a (3,+1) ring critical point between the N and methyl ligand. The absolute values of $\nabla^2\rho$ at the critical point of the Co−N and N−O bonds in **4** are smaller by 0.51 and 0.24 than those in **2**. Thus, the multiple bond character between the Co and N atoms (Co=N=O) of **2** is reduced because of the distortion of the nitrosyl group.

The Laplacian of the charge density of **TS(d)** is very different from that of **TS(a)** (Figure 5b). Although a new bond critical

Table 3. The Charge Density (ρ) on the Atoms[a] and Critical Points[b] and Laplacian of the Charge Density ($\nabla^2\rho$) at the Critical Point between the Bonded Atoms[b] Involved in Mechanism II

	4		TS(d)		5b	
	ρ	$\nabla^2\rho$	ρ	$\nabla^2\rho$	ρ	$\nabla^2\rho$
Co	16.312		16.428		16.559	
N	5.261		5.127		5.159	
C	4.640		4.315		4.184	
O	6.262		6.380		6.345	
P	4.683		4.720		4.725	
Co−N	0.149	0.617	0.148	0.511	0.133	0.957
Co−C	0.097	0.145	0.032	0.147	0.053	*0.217*
N−C	0.010	*0.036*	0.127	0.012	0.218	−0.398
N−O	0.405	−0.717	0.374	−0.427	0.352	−0.288

[a] Mulliken charge density at the RHF level for the atom, in which the core electrons are not included (units at the atomic sites are electrons). [b] The values of $\nabla^2\rho$ at the (3,+1) ring critical point are given in italic underline characters, other points are (3,−1) bond critical points (units of ρ = e/au^3 and $\nabla^2\rho$ = e/au^5).
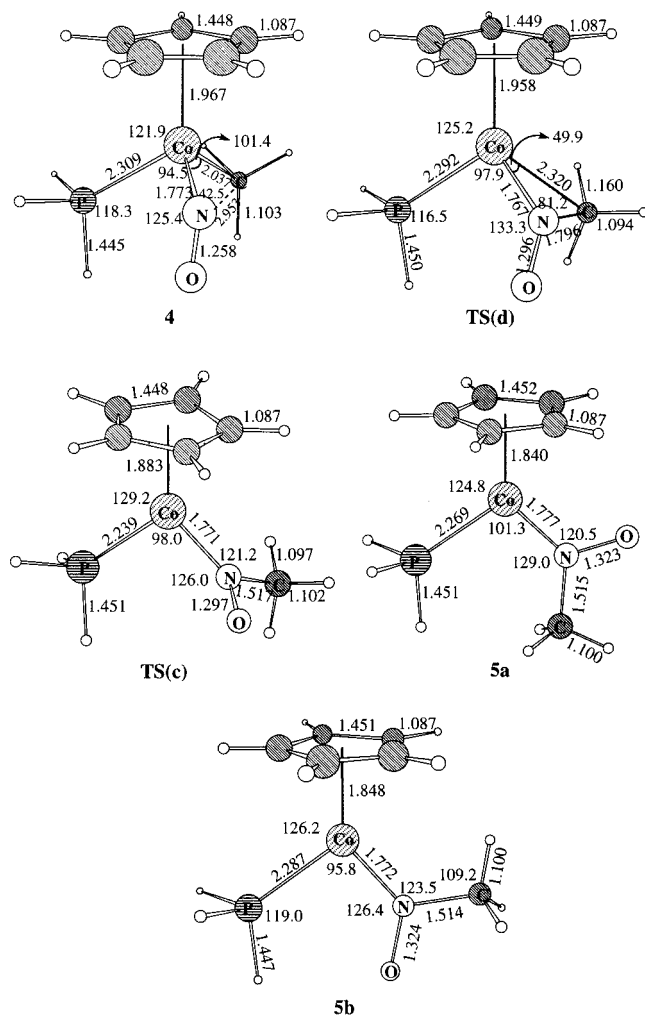
Figure 4. The DFT-B3LYP optimized geometries of the intermediate 4, insertion transition state **TS(c)** and **TS(d)**, products **5a** and **5b** (only the average C−C and C−H distances be given for the Cp ring).

point appears between the N and C atoms, a bond critical point remains between Co and C atoms, a result which suggests that the Co−C bond is not yet broken. A charge density analysis of **TS(d)** at the RHF level (see Table 3) shows that the charge densities at the C (methyl), N atoms, and the critical point of the N−O bond decrease by 0.325, 0.044, and 0.031 with respect to 4, respectively. Meanwhile, the charge densities at the Co and O atoms and the critical point between the N and C atoms increase by 0.117, 0.118, and 0.116 with respect to 4, respectively. However, the change in the charge density at the critical

Scheme 3
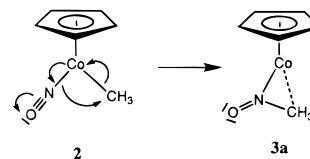
Scheme 4
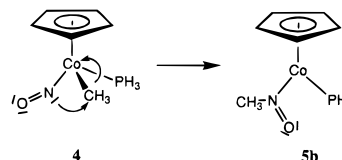
point of the Co−N bond is very small. Although the charge density at the bond critical point between the Co and C atoms of **TS(d)** decreases by 0.065 with respect to 4, the value of $\nabla^2\rho$ is nearly unchanged. Thus, a weak bond remains between the Co and C atoms in **TS(d)** and electron transfer occurs from the Co−C lone pair to the metal center rather than directly to the N−C bond. Thus, one can say that in **TS(d)** the Co−C bond is nearly broken and the charge densities of the C (methyl) and N atoms and the Co−C bond shift to the Co and O atoms and the N−C bond.

In Figure 5c the Laplacian of the charge density for **5b** displays a stronger shared interaction along N−CH$_3$ bond path. Compared with **TS(d)**, the value of $\nabla^2\rho$ for **5b** at the critical point of the Co−N bond obviously increases and that at the critical point of the N−O bond decreases. Thus, the Co−N bond of **5b** is apparently stronger than that of 4 or **TS(d)**. In this stage of the reaction (**TS(d)** to **5b**), the charge densities at the C (methyl) and O atoms and at the critical points of N−O bond decrease by 0.131, 0.035, and 0.022, respectively, while the charge densities at the Co, N atoms and the critical point of the N−C bond increase by 0.131, 0.032, and 0.091. However, the change in the charge density at the critical point of the Co−N bond is again very small. The charge density transfers from the C (methyl) and O atoms and N−O bond to the Co atom and the N−C bond. Thus, the Co atom plays an electron acceptor role in the late stage. Overall, along Mechanism II the Co−C bond is broken, and the N−C bond is formed late in the reaction as shown in Scheme 4.

Energies. Relative energies at the DFT-B3LYP and CCSD levels for the reactants (1 and 2), intermediate (4), transition state (**TS(d)** and **TS(c)**), and products (**5a** and **5b**) are given in Table 2. The profiles of the potential energy surfaces for Mechanism II are displayed in Figure 6. The intermediate 4 is more unstable by 16 and 18 kcal/mol than the reactants (1 and 2) at the DFT-B3LYP and CCSD levels, respectively. The experiments of Weiner and Bergman showed that replacing PPh$_3$ with PEt$_3$ causes significant stabilization of the bent-nitrosyl intermediate (4). Since PH$_3$ is a poorer nucleophile than either PPh$_3$ or PEt$_3$, the binding energy between the PH$_3$ ligand and CpCo(CH$_3$)NO should be smaller than that for the PPh$_3$ or PEt$_3$. Therefore, the calculated endothermicity for PH$_3$ is reasonable. The activation energy from 4 to 5 was calculated at the DFT-B3LYP and CCSD levels to be 19 and 34 kcal/mol. This means that the reaction from the reactants (1 and 2) to product 5 via Mechanism II occurs with very high barriers: 35−52 kcal/mol of 1 and 2 go to **TS(d)** in a single step and 19−34 kcal/mol if 4 is stable. The larger Δ value (difference between DFT and CCSD) for **TS(d)** may be due to multireference character arising from an "orbital crossing" (discussed below).

Therefore, with some confidence we can predict that the conversion of the reactants 1 and 2 through the bent nitrosyl
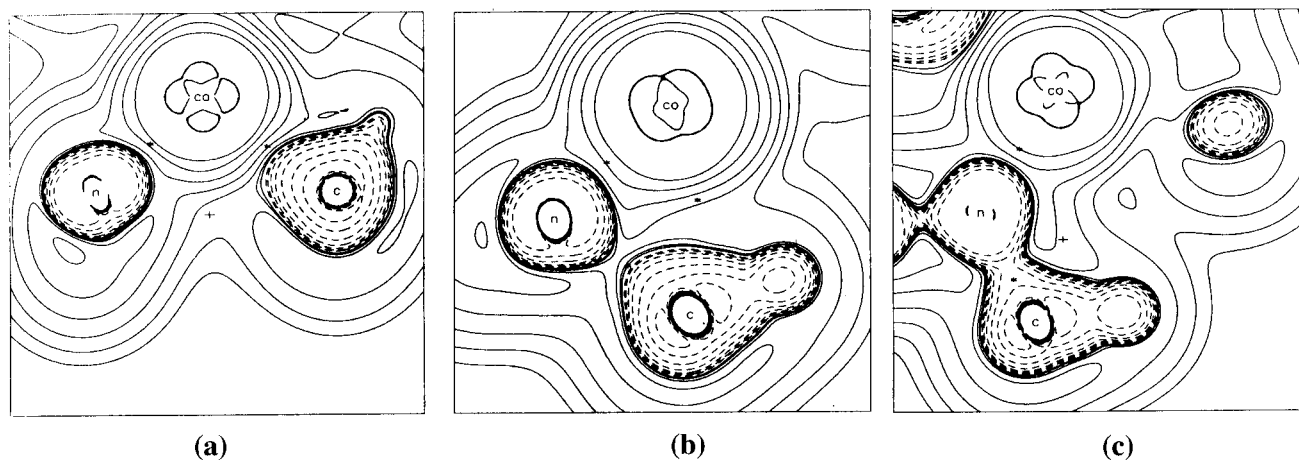
Figure 5. Contour plots of $\nabla^2\rho$ for the three structures along Mechanism I: (a) **2**, (b) **TS(a)**, and (c) **3a**. Contour parameters are the same as in Figure 2.
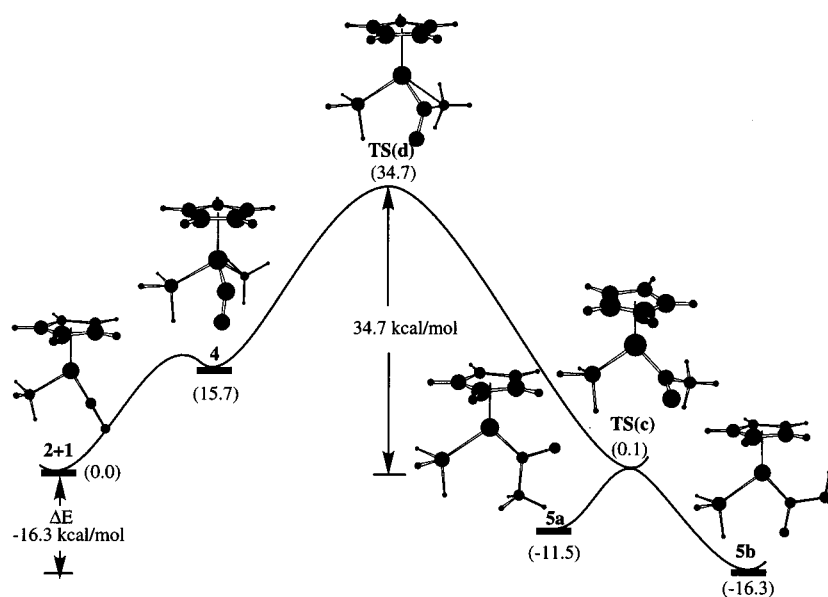

Figure 6. The profiles of the potential energy surfaces at the DFT-B3LYP level for Mechanism II (CCSD energies are given in Table 2).

adduct intermediate **4** then over the transition state **TS(d)** to the insertion product **5** will be much slower than the reaction via the path involving dissociation of the phosphine from **4** and the product formation by Mechanism I.

Molecular Orbital Analysis of the Migratory-Insertion Reaction in the Mechanisms I and II. According to our DFT and ab initio MO calculations, the insertion process would be the rate determining step in both Mechanism I and II. To elucidate the difference in the insertion between Mechanism I and Mechanism II and the origin of the higher barrier for II, we have analyzed qualitative MO diagrams and charge distributions for electronic features of the migratory-insertion process via these two mechanisms.

Insertion of NO into the Co$-$CH$_3$ σ Bond in the Mechanism I. To characterize the electronic structure of the insertion reaction along Mechanism I, we adopt the fragment MO approach.[34] The interactions between the valence MOs of the CpCo fragment (**6**) and the ligands (**7**), CH$_3^-$ and NO$^+$, give the nitrosyl methyl complex **2** (shown in the left-hand side of Figure 7), and those between the valence MOs of the CpCo

fragment (**6**) and N(O)CH$_3$ fragment (**8**) give the methylnitroso complex **3a** (shown in the right-hand side of Figure 7). In Figure 7 we display only those valence MOs that are involved in the stabilizing interactions. The stabilizing interactions in the nitrosyl methyl dcomplex **2** result from (i) the σ-bonding interactions between unoccupied MOs, p$_z$, d$_{yz}$, of **6** and the lone-pair orbital of NO, (ii) the σ-bonding interactions between unoccupied MOs, d$_{yz}$, p$_z$, of **6** and the lone-pair orbital of CH$_3^-$, and (iii) the back-bonding interaction between the high-lying d$_{xz}$ of **6** and the low-lying $\pi^-$$_o$ orbital of NO. The stabilizing interactions in the methylnitroso complex **3a** result from (i) the σ-bonding interactions between unoccupied MOs, p$_z$, d$_{yz}$, of **6** and the lone-pair orbital of **8**, P$_N$, and (ii) the weak back-bonding interaction between the high-lying doubly occupied d$_{xz}$ of **6** and the low-lying $\pi^-$$_o$ orbital of **8**. As the nitrosyl ligand "rotates" from **3a** to **3b** there is an in-phase overlap between d$_{yz}$ and the O component of the P$_N$ MO as illustrated in Scheme 2. It is also favorable for this P$_N$ MO to mix into the σ_{Co-N}. Thus, the stronger Co$-$O$-$N three-center interaction in **3b** stabilizes that species.

(31) (a) Dwoodi, Z.; Green, M. L. H.; Mtetwa, V. S. B.; Prout, K.; Schultz, A. J.; Williams, J. M.; Koetzle, T. F. *J. Chem. Soc., Dalton Trans.* **1986**, *802*, 1629. (b) Dwoodi, Z.; Green, M. L. H.; Mtetwa, V. S. B.; Prout, K. *J. Chem. Soc., Chem. Commun.* **1982**, *802*, 1410.
(32) (a) Butler, I. S.; Basolo, F.; Pearson, R. G. *Inorg. Chem.* **1967**, *6*, 2074. (b) Green, M.; Westlake, D. J. *J. Chem. Soc. (A)* **1971**, 367.

(33) Connor, J. A.; Zafarani-Moattar, M. T.; Bickerton, J.; El-Saied, N. I.; Suradi, S.; Carson, R.; Al Takhin, G.; Skinner, H. A. *Organometallics* **1982**, *1*, 1166.
(34) Albright, T. A.; Burdett, J. K.; Whangbo, M. H. *Orbital Interactions in Chemistry*; Wiley: New York, 1985.
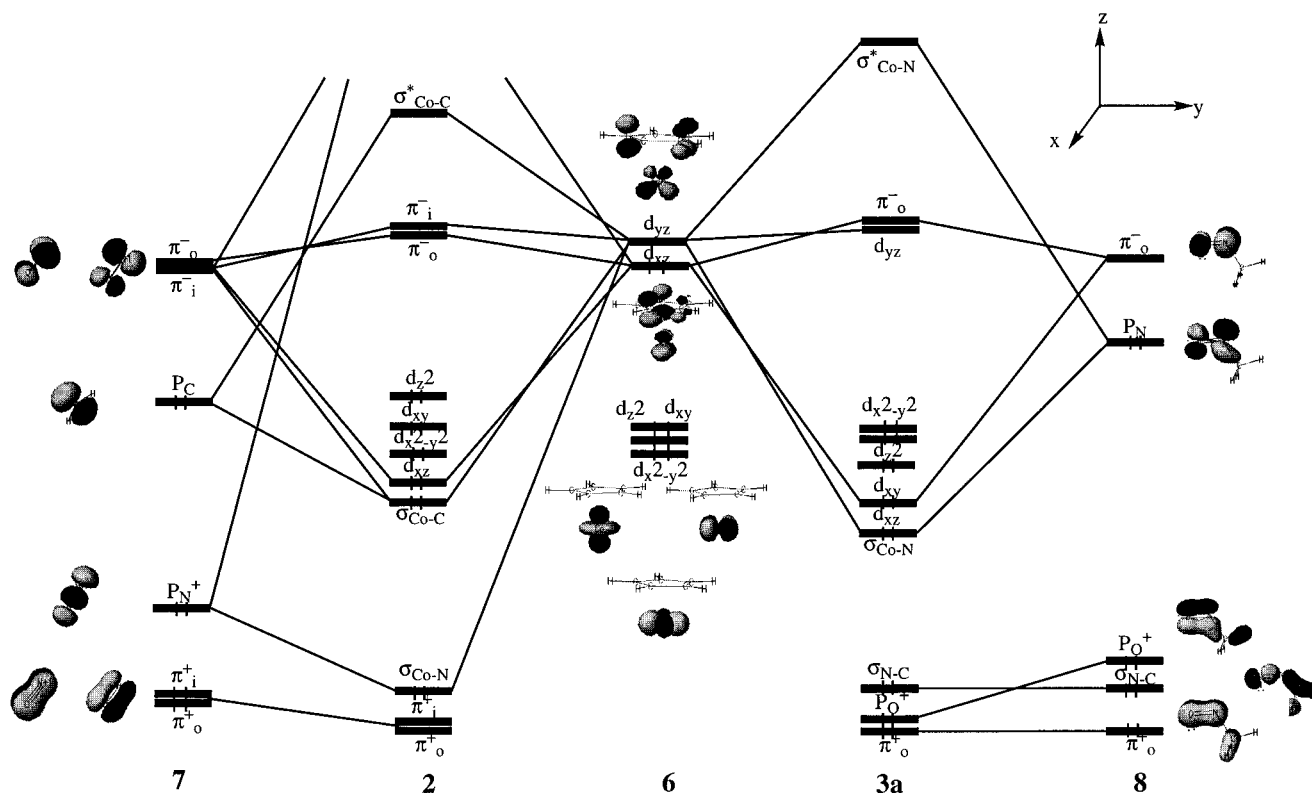
Figure 7. Simplified interaction diagrams for the interaction between CpCo (**6**) and the ligands (**7**), CH_3^-, NO^+ to the nitrosyl methyl complex **2** (the left-hand side) and for the interaction between CpCo (**6**) and N(O)CH₃ (**8**) fragment to the η^1-methylnitroso complex **3a** (the right-hand side).

In Figure 7 one can see that the nitrosyl methyl complex (**2**), and both the η^1- and η^2-intermediate complexes (**3**) are d^8 ($d_{xz}^2 d_{xy}^2 d_{x^2-y^2}^2 d_{z^2}^2 d_{zz}^0$) complexes. Therefore, the migratory-insertion reaction via Mechanism I preserves the d^8 orbital structure of the complex. Complex **3** differs from **2** by having a much lower-lying unoccupied d_{yz} orbital, which is available to interact with the lone-pair MO of the PH₃ ligand to form the stable complexes **5**.

To understand the electronic structures of the migratory-insertion process, in Figure 8 we display a Walsh diagram along the reaction path of Mechanism I from **2** through **TS(a)** to **3a**. The phase relationships of the occupied MOs in **2** and **3a** suggest smooth transformations of the N—O π bond, Co—C, and Co—N σ bonds of **2** to a lone pair of the O atom, the Co—N, and N—C σ bonds of **3a**. Meanwhile, the unoccupied MOs, π^-_i and σ^*_{Co-C}, of **2** transform to the MOs, d_{yz} and σ^*_{N-C}, of **3a**. It seems that the insertion reaction undergoes two stages. In the early stage of the insertion, as the nitrosyl group bends and the methyl ligand migrates, the Co—C σ bond and N—O in-plane π bond are weakening. The charge density of the Co—C bond of **2** transfers through the metal center to the N—O in-plane π antibond (for a new Co—N bond) of **Ts(a)**, while the charge densities of the N—O in-plane π bond and Co—N bond of **2** shift to the O atom (for a new lone pair) and to the N—C bond of **TS(a)**. It is clear that such transformations facilitate the Co—C bond-breaking as well as the nitrosyl bending to form new Co—N and N—C bonds. In the late stage of the insertion, as the nitrosyl group bends further and inserts, charge density transfers to the N—C bond from the N atom, the original Co—N bond, and the C (methyl) atom. Meanwhile, the charge density of a lone pair of the O atom shifts to the new Co—N bond. This charge density reorganization facilitates the formations of the new N—C bond and Co—N bonds. According to the changes in the charge densities (see above), one can conclude the Co center plays a critical dual role as electron acceptor and electron donor in the migratory-insertion. The charge density of the Co—C bond, through the metal center, easily transfers to
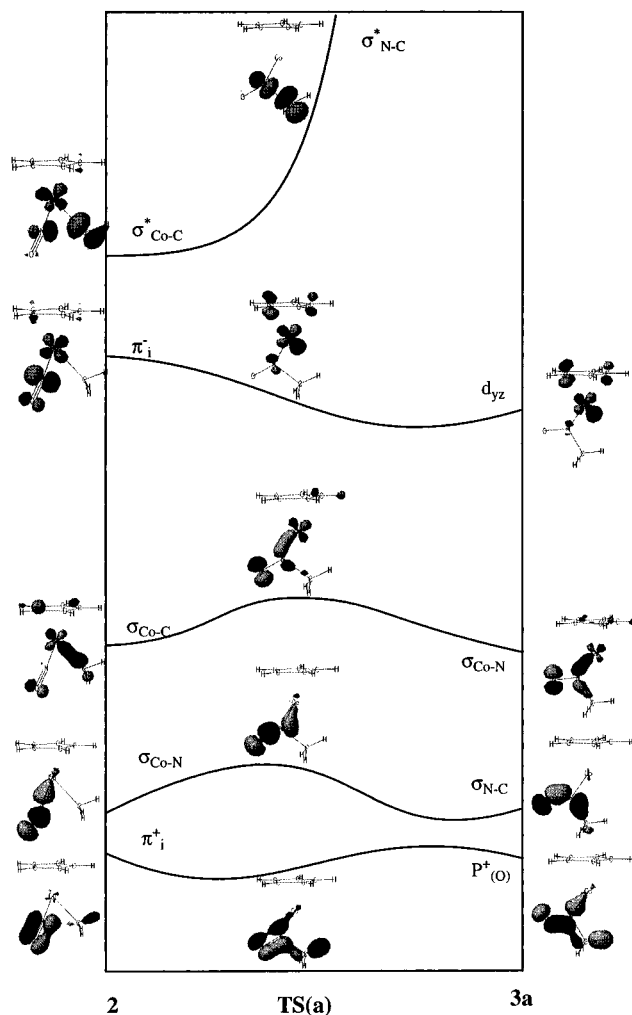

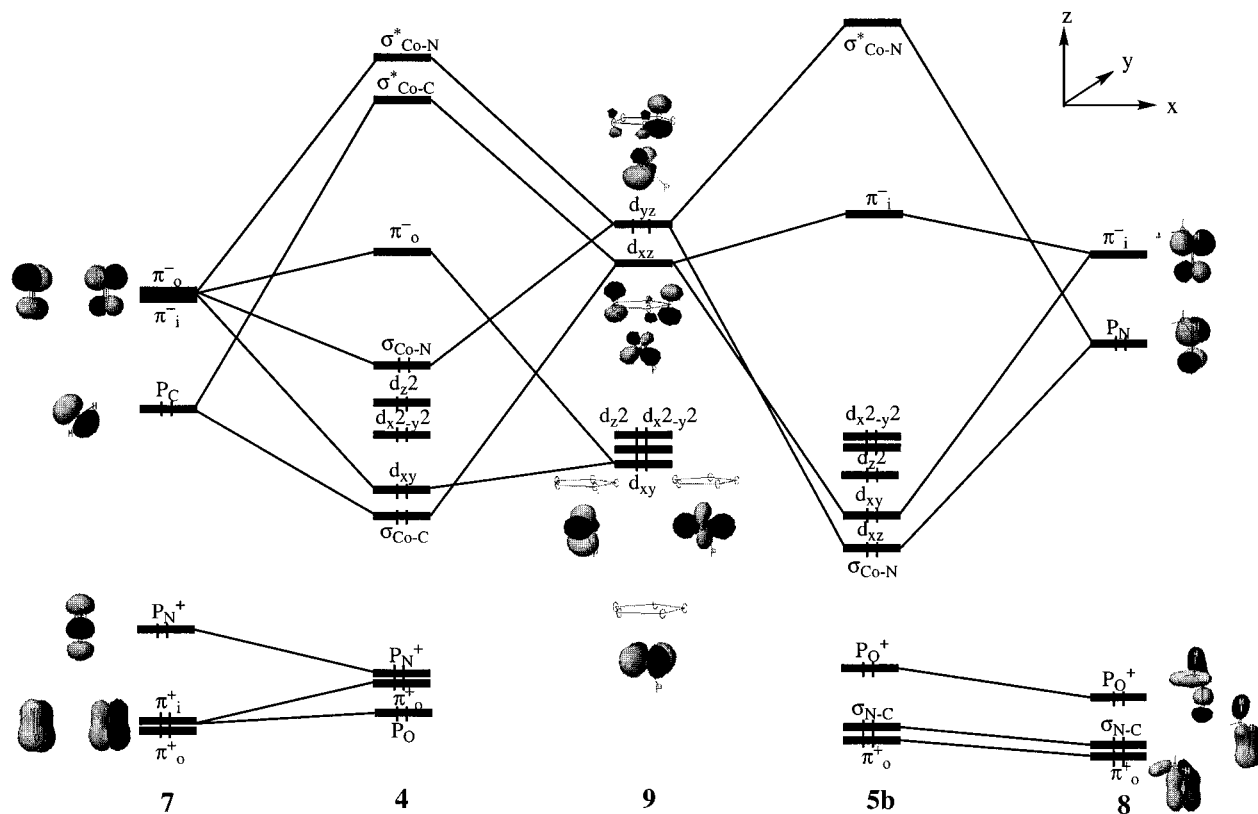**Figure 8.** Walsh diagram for the insertion reaction via Mechanism I from **2** through **TS(a)** to **3a**.

Figure 9. Simplified interaction diagrams for the interaction between CpCoPH$_3$ (**9**) and **7** to the bent-nitrosyl methyl complex **4** (the left-hand side) and for the interaction between CpCoPH$_3$ (**9**) and **8** to the methylnitroso complex **5b** (the right-hand side).

the N–O π_i^- bond forming the new Co–N σ bond. Thus, the ability of the metal center to perform both functions lowers the activation energy of the migratory-insertion reaction.

Insertion of NO into the Co–CH$_3$ σ Bond in the Mechanism II. Similarly, in this section we have adopted a fragment MO approach,[34] concentrating on interactions between the valence MOs of the fragment CpCoPH$_3$ (**9**) and **7** and between the valence MOs of **9** and **8**. Figure 9 shows how the five d orbitals of **9** interact with orbitals of **7** and **8**, respectively. The interaction diagram for the intermediate **4** is illustrated in the left-hand side of Figure 9. The high-lying, nearly degenerate, MOs of **9**, d$_{yz}$ and d$_{xz}$, interact with the low-lying MOs of **7**, π_i^- of NO$^+$ and P$_C$ of CH$_3^-$, respectively. Here, we have doubly occupied the d$_{yz}$ and left the d$_{xz}$ unoccupied to prepare the fragment for bonding. The high-lying σ_{Co-N} and the low-lying σ_{Co-C} orbitals of **4** are formed by these interactions. In addition, a weak back-bonding interaction occurs between the occupied d$_{xy}$ orbital of **9** and unoccupied π_o^- orbital of NO. The MOs of **4**, P$_N^+$, P$_O^+$, and π_o^+, represent the lone pair N, lone pair O, and N–O π bond, respectively. The MOs interaction diagram for the product **5b** is shown in the right-hand side of Figure 9. The MOs of **5b**, P$_O^+$, σ_{N-C}, and π_o^+, represent the lone pair O, N–C σ, and N–O π bonds. A low-lying Co–N σ bond of **5b** is formed by the interaction between a high-lying MO of **9**, d$_{yz}$, and a low-lying lone pair N orbital of **8**, P$_N$. A low-lying MO of **9**, d$_{xz}$, interacts with a high-lying N–O π anti-bond orbital of **8**, π_i^-, which leads to a strong back-bonding interaction in **5b**. It is obvious that the interaction between **9** and **7** results in a d^6 (d$_{xy}^2$d$_{x^2-y^2}^2$d$_{z^2}^2$d$_{xz}^0$d$_{yz}^0$) complex **4** and that the interaction between **9** and **8** leads to a d^8 (d$_{xz}^2$d$_{xy}^2$d$_{x^2-y^2}^2$d$_{z^2}^2$d$_{yz}^0$) complex **5b**. Therefore, the migratory insertion reaction via Mechanism II actually converts a d^6 complex to a d^8 complex.

In Figure 10 we display the Walsh diagram along the reaction path of Mechanism II, going from the intermediate, **4**, through a transition state, **TS(d)**, to the product, **5b**. When the methyl

group moves toward the nitrosyl group and the Co–C bond breaks, the σ_{Co-N}, σ_{Co-C}, and P$_N^+$ orbitals of **4** can be correlated with the σ_{Co-N}, d$_{xz}$, and σ_{N-C} orbitals of **5b**. In the early stage, the energy of the σ_{Co-C} orbital rises and the energy of the σ_{Co-N} orbital falls. Meanwhile, the original σ^*_{Co-N} and π_o^- levels are stabilized because of the structural distortion, and the σ^*_{Co-C} level is destabilized strongly because of mixing with the N and gaining strong N–C σ anti-bonding character. As the bent NO ligand rotates and the methyl ligand migrates, at the saddle point the metal–carbon σ-bond character of the σ_{Co-C} orbital is diminishing as the charge densities of the C atom and the Co–C bond shift to the σ^*_{Co-C} and π_o^- levels. It means that the σ_{Co-C} orbital becomes a Co d$_{xz}$ orbital, in which there is the strong Co–N anti-bonding character. Thus, this mechanism (II) is clearly different from Mechanism I; here, the charge density transfer from the Co–C σ bond to the metal center and N atom requires a greater energy. The donation of the Co–C pair to the metal is more difficult because the bent NO (already NO$^-$) is poorer at accepting charge density from Co because it would be forced toward NO^{3-}. Meanwhile, the N–CH$_3$ bond is forming as the charge density of the lone pair on the N atom transfers to the N–C bond. Therefore, in the migratory step of the migratory-insertion reaction of Mechanism II the charge densities of the metal center and N–C bond originate from the Co–C bond and the lone pair on the N atom. In the later stage of the insertion reaction, the σ_{Co-N} orbital smoothly correlates to Co–N σ-bond, while the original lone pair electrons (P$_N^+$) on the N atom completely transfers to the N–C σ-bond of the methylnitroso ligand. It results in the new Co–N and N–C bonds formed. Meanwhile, the nitrosyl π^* orbital (original π_o^-) clearly mixes with the destabilized metal orbital so that the d$_{xz}$ level is ultimately stabilized by metal-nitrosyl π bonding. Thus, these latter changes result in electron density shifting from the original nitrosyl ligand to the metal center and the N–C bond. Overall, the metal center plays an acceptor role as it returns to d^8 from **4** to **5b**.
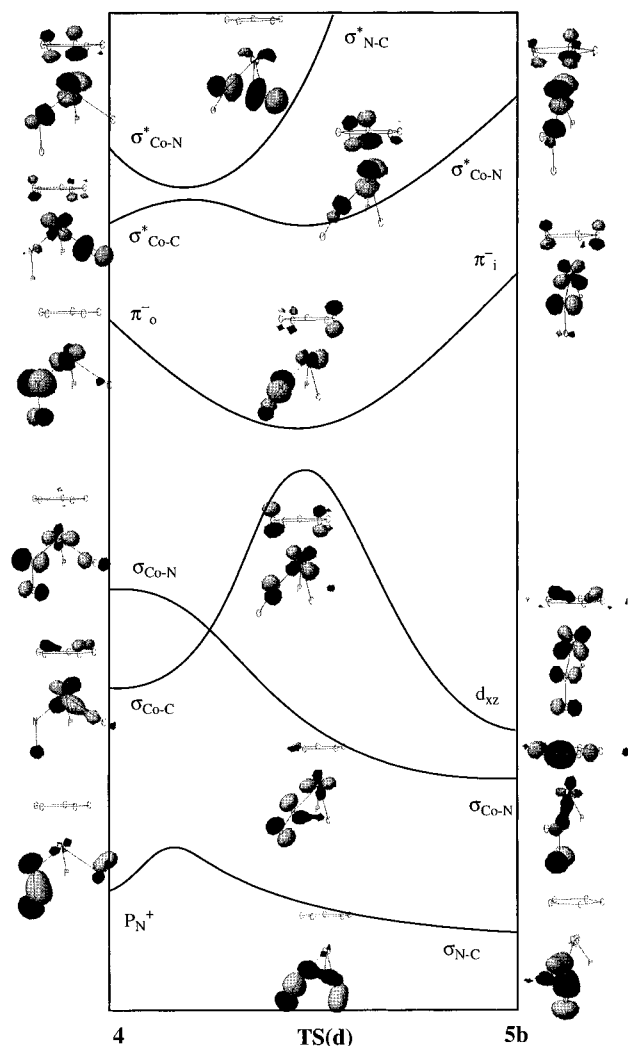
Figure 10. Walsh diagram for the insertion reaction via Mechanism II from **4** through **TS(d)** to **5b**.

Conclusions

Both DFT and ab initio energy profiles of NO insertion into the Co−CH$_3$ σ bond show that the migratory-insertion step is the rate-determining step for both Mechanisms I and II. The migratory-insertion without PH$_3$ association (Mechanism I) occurs with a lower activation energy of 10−20 kcal/mol. Although the methylnitroso intermediate is endothermic by 8−17 kcal/mol, the overall reaction is exothermic by −10 to −16 kcal/mol depended on the level of theory. Our results support mechanism I that even in the presence of PH$_3$ proceeds along a path in which PH$_3$ attack occurs late (**2** → **TS(a)** → **3a** → **5a** → **TS(c)** → **5b**), in good agreement with the kinetic experiment by Weiner and Bergman.

Charge density (ρ) and Laplacian ($\nabla^2\rho$) analysis at the RHF level and MO analysis of extended Hückel calculations reveal (i) that in the early stage of the migratory-insertion the metal center acts as an agent in the transfer of electron density from the methyl ligand to the nitrosyl group, a process which weakens the Co−C bond, and (ii) that in the later stage of the migratory-insertion the lone pair on the nitrosyl ligand attacks the methyl group forming the N−C bond. Thus, CH$_3$ migrates as "CH$_3^+$" in both mechanisms. Although Co plays a dual role as electron acceptor and donor in the early stage of the migratory-insertion reaction along both Mechanisms I and II, the actual electron transfer process is different. Along Mechanism I, it is very easy to transfer electron density from the original σ_{Co-C} bond through the original σ_{Co-N} bond to N−C bond due to the metal center remaining d^8. In contrast, for Mechanism II, the original σ_{Co-C} orbital must rise to high energy before it can transfer electron density to the d$_{xz}$ orbital of the product as it must convert the d^6 metal to d^8. The former process provides a lower energy path.